Polymer 51 (2010) 5172–5185

Contents lists available at ScienceDirect

Polymer

journal homepage: www.elsevier.com/locate/polymer

Novel in situ polydimethylsiloxane-sepiolite nanocomposites: Structure-property relationship

Nabarun Roy [a], Anil K. Bhowmick [a,b,*]

[a] Rubber Technology Centre, Indian Institute of Technology, Kharagpur 721302, India
[b] Indian Institute of Technology, Patna 800013, India

ARTICLE INFO

Article history:
Received 21 June 2010
Received in revised form
16 August 2010
Accepted 28 August 2010
Available online 6 September 2010

Keywords:
Polydimethylsiloxane
Sepiolite
Nanocomposites

ABSTRACT

A series of novel in situ polydimethylsiloxane (PDMS)-sepiolite nanocomposites were synthesized by anionic ring opening polymerization of octamethylcyclotetrasiloxane. These nanocomposites were characterized by Attenuated Total Reflection-Fourier Transform Infrared Spectroscopy, Wide Angle X-Ray Diffraction (WAXD), Transmission Electron Microscopy (TEM), mechanical and dynamic mechanical properties and thermogravimetry. This paper highlights the structure-property relationship of in situ PDMS-sepiolite nanocomposites and a way to improve the mechanical, dynamic mechanical and thermal properties of silicone rubber. Comparison of these physico-mechanical properties with those of the ex situ nanocomposites reflects greater degree of filler dispersion for the in situ nanocomposites. Increasing amount of the filler reduced the size of the crystalline domains in PDMS matrix, which was evident from the X-Ray and the dynamic mechanical analysis. However, the polymer-filler interaction was even more prominent to negate the effect of the deterioration of the properties due to decrease in size of the microcrystallites. The polymer-filler interaction was reflected in the improved mechanical and thermal properties which were the consequences of proper dispersion of the filler in the polymer matrix. The modulus improvement of the rubber-clay nanocomposites was examined by using Guth and Halpin-Tsai model. The temperature of maximum degradation was raised by 167 °C and improvement of 210% in tensile strength and 460% in modulus at 100% elongation was observed. These results were correlated with the data obtained from WAXD and TEM studies.

1. Introduction

Intricacy in properties and behavior of silicone rubber based nanocomposites has drawn the attention of researchers in recent years [1–4]. A large degree of flexibility, high thermal stability and low electrical conductivity accounts for its applicability in innumerable technological applications. Studies related to structure-property relationship of PDMS-silica nanocomposites have been done till date [5,6]. Thermal properties of the single walled carbon nanotube-silicone nanocomposites have been investigated [7]. Moreover, silicone rubber-nanoclay based composites have also gained importance in recent years due to improvement in their physico-mechanical properties [8,9]. However, there is no report on the in situ PDMS-layered silicate nanocomposites where polymerization is carried out with the monomer in presence of a filler. The problem for the preparation of these nanocomposites, as learnt from our initial studies was mainly due to curing by platinum catalyst and crosslinker with Si–H functionality, as the reaction for the synthesis of the polymer nanocomposites was catalyzed by a base. This problem was ultimately overcome by understanding the process chemistry. The key to this solution was obtained from the fact that Si–H bonds in the crosslinker are susceptible to bases and thus undergo dissociation [10].

Improvements in mechanical, thermal and barrier properties have been achieved by incorporation of low concentration of inorganic nanoparticulates in the polymer matrix. These improvements are even more than conventional macro- and micro-scale composites due to increased interaction at the polymer-filler interface for nanocomposites [8,9]. Extensive research has been carried out in our laboratory till date in the field of nanocomposites. Bhattacharya et al. quantified polymer-filler interaction by introducing Interface Area Function (IAF) [11]. On the other hand, Maji et al. showed that gas permeability for the PU-organoclay based nanocomposites decreases due to formation of tortuous pathways by the clay platelets which act as barriers in the path of the gas molecules [12].

* Corresponding author. Rubber Technology Centre, Indian Institute of Technology, Kharagpur 721302, India. Tel.: +91 3222 283180/612 2277380; fax: +91 3222 220312/612 2277384.
E-mail addresses: anilkb@rtc.iitkgp.ernet.in, director@iitp.ac.in (A.K. Bhowmick).

0032-3861/$ – see front matter © 2010 Elsevier Ltd. All rights reserved.
doi:10.1016/j.polymer.2010.08.064

Small-angle X-ray scattering (SAXS) and modulated DSC (MDSC) have been used as tools to quantify and correlate the effect of nanoclay platelets on the lamella order for poly[styrene-*b*-(ethylene-*co*-butylene)-*b*-styrene] triblock copolymer (SEBS) and polar modified SEBS based nanocomposites by Ganguly et al. [13]. A detailed analysis of the thermal degradation behavior of various rubber matrices such as SBR, BR and NBR filled with unmodified and organically modified clay has been made by Sadhu et al., who found that thermal stability as well as the thermal degradation pattern of the resultant nanocomposites depend entirely upon type of matrix and clay, their polarity and the clay concentration in the matrix [14]. It has been also demonstrated that in situ nanocomposites impart better properties than ex situ nanocomposites [15].

Clays have platelet structure with the individual plates having thicknesses of just a nanometer with high aspect ratio [16]. Nanocomposite formation generally leads to penetration of polymer chains into gallery gap of the clays, thereby separating individual platelets and leading to complete exfoliation of the clay [17].

Sepiolite is a 2:1 phyllosilicate having a fibrous morphology, unlike other similar clays, with one octahedral sheet sandwitched between two tetrahedral sheets [18]. Chemically, it is a hydrated magnesium silicate with the ideal formula $Si_{12}Mg_8O_{30}(OH)_4.8H_2O$. Its structure consists of narrow strips formed by two sheets of SiO_4 tetrahedrons bonded to a central sheet of magnesium atoms. Each strip is linked to the other by inversion of apical O atoms of the SiO_4 tetrahedrons [19]. Hence sepiolite is also called “inverted ribbons” [18]. Sepiolite has the surface area of about 300 m^2/g with a very high density of silanol groups and possesses fine micropore channel of the dimension 0.36 nm × 0.11 nm along the length of the fiber. Its remarkable absorptive and adsorptive properties, due to the high surface area and porosity, have been explored in preparation of polymer nanocomposites with improving processability, dimensional stability, mechanical strength and thermal resistance [20].

The polymer matrix used for study with sepiolite as the filler are polyester [20], nylon-6 [21], chitosan [22], poly(hydroxyethyl acrylate) [23], poly(sodium acrylate) [24], epoxy resin [25], and polypropylene [26]. In our laboratory, HNBR-sepiolite nanocomposites have been prepared by solution mixing by Choudhury et al. and the difference in their interaction parameters with various solvents has been analyzed for the first time [18]. However, effect of in situ synthesis of nanocomposites has not been studied till date to the best of our knowledge. Moreover, only a few preliminary investigations based on PDMS-sepiolite nanocomposites have been done [27,28]. In this work, for the first time, a high degree of dispersion of the sepiolite fibers has been achieved which has not been possible by conventional ex situ method of nanocomposite preparation and here lies the novelty of this work. The effect of better dispersion is reflected in mechanical, dynamic mechanical and thermal properties. This work makes the first attempt to analyze the structure-property relationship of in situ PDMS-sepiolite nanocomposites.

In this paper anionic ring opening polymerization of the cyclic siloxane monomer cyclotetrasiloxane has been carried out in presence of nanofiller. The synthesized nanocomposites were characterized by Attenuated Total Reflection-Fourier Transform Infrared Spectroscopy (ATR-FTIR), X-Ray Diffraction (XRD), Transmission Electron Microscopy (TEM), mechanical and dynamic mechanical properties and thermogravimetry. These results were compared with those of ex situ nanocomposites prepared by solution casting technique. This work highlights the significance of the extent of dispersion of nanofillers in determining improvement in physico-mechanical properties of the nanocomposites. The opposing effect of the polymer-filler interaction and the decrease in size of the microcrystalline domain in determining the mechanical, dynamic mechanical and thermal properties of the nanocomposites in comparison with the virgin polymer has been investigated in this paper.

2. Experimental

2.1. Materials

Octamethylcyclotetrasiloxane $[(CH_3)_2SiO]_4$ (D_4), Platinum catalyst (Pt catalyst in U-10, where U-10 is a vinyl PDMS system with molecular weight 74,400 and viscosity 10 Pa s having a hydride content of 0.05 mmol/g) and the hydride crosslinker polymethylhydrogenosiloxane (V430) with the chemical formula $Me_3Si(OSiMe_2)_x(OSiMeH)_yOSiMe_3$, where x and y are 10, having hydride content of 4.3 mmol/g were supplied by Momentive Performance Materials, Bangalore, India. D_4 having boiling point of 175 °C; viscosity of 1.396; density of 0.955 and purity >99% (GC) was freshly distilled before use.

1, 1, 3, 3- Tetramethyl-1,3-divinyldisiloxane (purity 97%) with a boiling point of 139 °C and density of 0.809, was supplied by Sigma–Aldrich, USA and used as received.

Potassium hydroxide was purchased from Merck, Mumbai, India.

Pangel B20 (Sepiolite clay) was obtained from Tolsa S.A., Spain. This is an organically modified sepiolite, which is chemically known as organically modified hydrated magnesium silicate, has >85% sepiolite clay and <15% quaternary ammonium salt.

Toluene was purchased from Merck, Mumbai, India and used as received.

2.2. Synthesis of pristine PDMS and PDMS-based nanocomposites

2.2.1. Synthesis of vinyl terminated PDMS

15g (0.05 mole) of D_4 was distilled in order to remove the Si–H and Si–OH containing species. This was taken in a three necked round-bottomed flask fitted with a condenser, a thermometer jacket for regulating the temperature and an arrangement containing an inlet and outlet for nitrogen. 0.08 g (0.5%) of KOH was finely grinded in nitrogen atmosphere and was introduced into the flask. The temperature of the bath was gradually raised up to 140 °C and was made constant at this temperature. Within 15 min, the KOH got dissolved into the liquid monomer followed by a gradual increase in viscosity of the mixture. The reaction was continued for 2 h which led to a tremendous increase in the viscosity of the material within the reaction vessel. 0.05 g (2×10^{-4} mole) of 1, 1, 3, 3 − Tetramethyl-1,3-divinyldisiloxane was added to the viscous mass and the reaction was continued for another two more hours at the same temperature. The addition of the 1, 1, 3, 3 − Tetramethyl-1,3-divinyldisiloxane was followed by fall in viscosity of the resultant mixture. At the end of 4 h of the reaction, the resultant mixture was left overnight for complete chain termination.

2.2.2. Work up of the vinyl terminated PDMS

The vinyl terminated PDMS synthesized contained unreacted KOH. The synthesized polymer was dissolved in toluene. This was neutralized by adding H_3PO_4 drop wise and stirred vigorously with a glass rod and the pH of the resulting solution was detected using pH paper. The solution was left to stir for overnight for complete neutralization and precipitation of the salt generated.

2.2.3. Curing reaction of vinyl terminated PDMS

13 g of the synthesized polymer was dissolved in 50 ml of toluene. To this homogeneous solution 0.05 g of Pt catalyst and 25 ml of trichloroethylene were added and dissolved. This constituted one part of the curing system. Another part consisted of 0.32 g of Si–H crosslinker dissolved in 10 ml of toluene. These two parts

were mixed thoroughly and the resulting solution was degassed for 5 min to remove dissolved gases, if any, from the solution. The degassed solution was poured into a Teflon petridish and left undisturbed overnight. The evaporation of the solvent gave a transparent sheet of the cured PDMS with uniform thickness of 0.5 mm which was subjected to a temperature of 80 °C for complete curing in presence of vacuum.

2.2.4. Synthesis of in situ PDMS-sepiolite nanocomposites

A calculated amount of filler was soaked in 15 g of D_4 (0.05 mole) and was left overnight for the monomer to get soaked into the narrow channels of the filler so that polymerization could occur over there. This was sonicated for 15 min before the reaction. To this, the same amount of base and vinyl terminator was added and polymerization was carried out under same reaction conditions. Work up and curing of the nanocomposites were carried out in exactly the same way as that of pristine PDMS. The details of the nanocomposites preparation are tabulated in Table 1.

2.2.5. Synthesis of ex situ PDMS-sepiolite nanocomposites by solution casting

15 g of D_4 and 0.08 g of KOH were taken in a three necked round-bottomed flask and polymerization was initiated in nitrogen atmosphere. After 2 h 0.05 g of the vinyl terminator was added to the reaction mixture and the reaction was terminated after 2 h of the vinyl terminator addition. The reaction mixture was left overnight.

This was neutralized with required amount of H_3PO_4 after dissolution in toluene. Calculated amount of sepiolite was dispersed in toluene and sonicated for 15 min. This was then added to the polymer solution and stirred for 2 h. To the resulting solution, curing agent was added, the mixture was degassed, cast in Teflon petridish and left overnight for curing at room temperature.

2.3. Instrumentation

2.3.1. Characterization of synthesized PDMS

2.3.1.1. Number average molecular weight. Number average molecular weight was determined using end group analysis. For this purpose ^{29}Si Nuclear Magnetic Resonance (NMR) spectra of neat vinyl endcapped PDMS was taken using Bruker AM-360, 400 MHz NMR spectrometer. The concentrations of samples prepared were 50% w/v in $CDCl_3$ solution. The internal standard used was tetramethylsilane (TMS). A heteronuclear gated decoupled pulse sequence (NONOE) was used to acquire ^{29}Si NMR spectra. A paramagnetic relaxation agent such as chromium acetylacetonate was added to ensure exact integration.

2.3.2. Characterization of nanocomposites

2.3.2.1. Wide-angle X-ray diffraction (WAXD) (in low angle range). The Wide Angle X-ray diffraction patterns of the samples were recorded in a Philips X-ray diffractometer (model PW-1710) using crystal monochromated Cu Kα radiation in the angular range 2–9° (2θ) and at 40 kV operating voltage and 20 mA current.

2.3.2.2. Transmission electron microscopy (TEM). The samples for TEM analysis were prepared by ultra-cryomicrotomy with a Leica Ultracut UCT (Leica Microsystems GmdH, Vienna, Austria). Freshly sharpened glass knives with cutting edges of 45° were used to obtain cryosections of about 100–150 nm thickness at −150 °C. The cross sections were collected individually in sucrose solution and directly supported on a copper grid of 300 mesh. Microscopy was performed with JEOL 2100, Japan. Transmission electron microscope was operated at an accelerating voltage of 200 kV.

2.3.2.3. Attenuated total reflection-Fourier transmission infrared (ATR-FTIR) spectroscopy. Attenuated total reflection (ATR)-Fourier transmission infrared spectra (FTIR) spectra of the samples were taken using an infrared spectrophotometer (Nicolet Nexus, Madison, WI, USA) within a range of 650 cm^{-1} to 4000 cm^{-1} taking a resolution of 4 cm^{-1}. ZnSe prism was used for ATR-IR spectroscopy measurements. An average of 120 scans was reported for each spectrum.

2.3.2.4. X-ray diffraction (XRD) studies in wide angle range. The Wide Angle X-ray diffraction patterns of the samples were recorded in a Philips X-ray diffractometer (model PW-1710) using crystal monochromated Cu Kα radiation in the angular range 10–70° (2θ) and at 40 kV operating voltage and 20 mA current. The d value was obtained from the Bragg's equation:

$$n\lambda = 2d\sin\theta \quad (1)$$

where, n = 1, λ = wavelength of the X-ray used and θ = half the Bragg's angle. The crystallite size was calculated according to the Scherrer equation [29]:

$$L_{hkl} = K\lambda/\beta\cos\theta \quad (2)$$

where, L_{hkl} refers to the size of the crystallites at reflection of *hkl*, K is the Scherrer factor and β is the full width at half maximum.

2.3.2.5. Dynamic mechanical analysis (DMA). The dynamic mechanical data of the samples (12.59 mm × 6.65 mm × 1.2 mm) were obtained by using a DMA of TA instruments (model Q800). The sample specimens were analyzed in tensile mode at a constant frequency of 1 Hz, a strain of 0.05% and a temperature range from −130 to 50 °C at a heating rate of 3 °C/min. The data were analyzed by TA Universal analysis software on a TA computer attached to the machine. Storage modulus (E') and loss tangent (tan δ) were measured as a function of temperature for all the samples under identical conditions. The temperature corresponding to the peak in

Table 1
Preparation of samples with designations (PDMS-sepiolite nanocomposites).

Samples	D_4 used (g)	KOH (g)	Vinyl terminator (g)	Polymer obtained (g)	Amount of Crosslinker (g)	Amount of Sepiolite (with respect to the polymer obtained) (phr)
vp s0	15	0.08	0.05	13	0.32	_
vp s2	15	0.08	0.05	13	0.32	2
vp s4	15	0.08	0.05	13	0.32	4
vp s6	15	0.08	0.05	13	0.32	6
vp s8	15	0.08	0.05	13	0.32	8
vp s10	15	0.08	0.05	13	0.32	10
[a]VP S4	15	0.08	0.05	13	0.32	4
[a]VP S8	15	0.08	0.05	13	0.32	8

phr: Parts per hundred gram of rubber.
[a] VP S4 and VP S8 stand for the ex situ prepared nanocomposites by solution casting technique.

tanδ versus temperature plot was taken as the glass–rubber transition temperature (T_g).

2.3.2.6. Mechanical properties. Tensile specimens ASTM D 412-98 were punched out from the molded sheets using ASTM Die-C. The tests were carried out on a Zwick UTM, Model – Z010 (Zwick GmbH and Co., Ulm, Germany) at a cross-head speed of 500 mm/min at 25 °C. The average of three tests is reported here. The errors of the tensile and elongation at break measurements were ± 1%.

2.3.2.7. Thermogravimetric analysis (TGA). The TGA analysis was carried out in Perkin Elmer Instrument, Diamond TG-DTA, at the heating rate of 20 °C/min under nitrogen atmosphere up to 800 °C. The data were analyzed by TA Universal analysis software on a TA computer attached to the machine. A small amount of material (around 5 mg) was used for the TGA study. The analysis of the Thermogravimetric (TG) and derivative thermogravimetric (DTG) curves was done in oxygen and the onset temperature, weight loss at major degradation steps and temperature corresponding to the maximum value in the derivative thermogram were recorded. The temperature at which maximum degradation takes place is denoted by T_{max} and onset temperature of degradation is denoted by T_i. The error in the measurement was ± 1 °C.

3. Results and discussion

3.1. Properties of pristine PDMS

3.1.1. Synthesis of vinyl terminated PDMS and mechanism of the curing reaction

Polydimethylsiloxane was synthesized following the principle of anionic ring opening polymerization of octamethylcyclotetrasiloxane [30]. The scheme of polymerization is shown in Fig. 1. Curing of the resultant polymer was carried out using the principle of hydrosilylation. The crosslinked material was found insoluble in toluene, thereby suggesting complete three-dimensional network formation. Mechanism of platinum catalyzed hydrosilylation reaction was proposed by Chalk and Harrod [31]. Catalytic cycle of the platinum catalyzed curing reaction of room temperature vulcanizate is depicted in Fig. 2.

3.1.2. Number average molecular weight (M_n)

On the basis of end group analysis [32], it is possible to determine the number average molecular weight (M_n) of the polymer by ^{29}Si NMR spectroscopy. Fig. 3 shows the ^{29}Si NMR spectra of synthesized vinyl PDMS. The signals at 0, −4, and −21 correspond to TMS, Si–vinyl, and Si–O–Si (backbone), respectively. The number of silicon atoms attached to the vinyl end groups, N_{vin} was

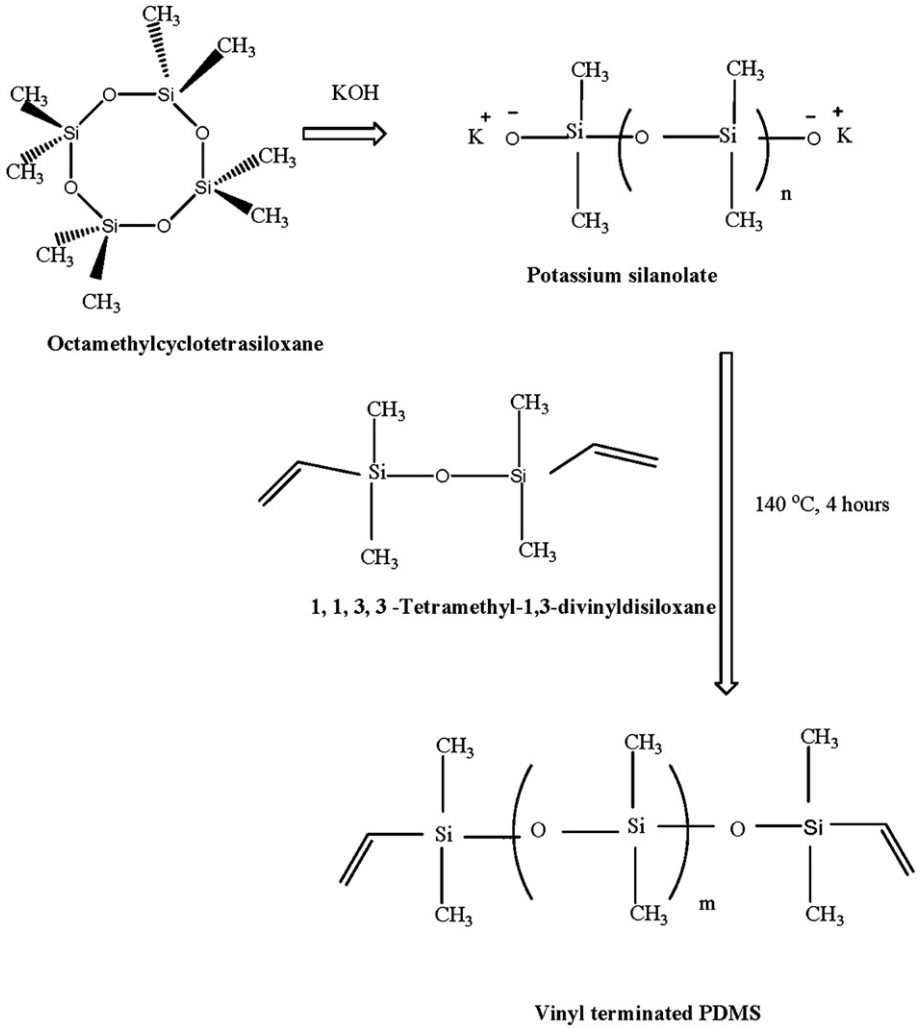

Fig. 1. Scheme of the polymerization reaction.

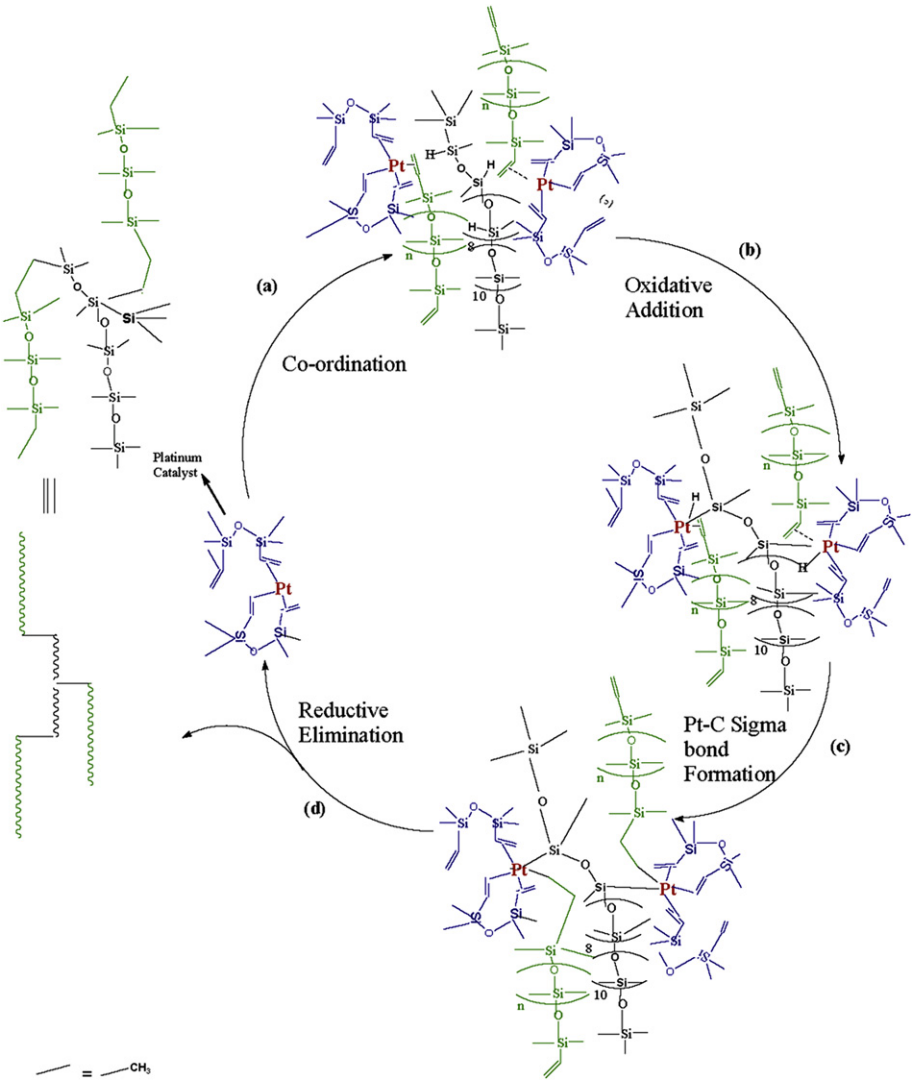

Fig. 2. Catalytic cycle for the curing reaction of vinyl terminated PDMS.

determined by integration of the peak for silicon attached to vinyl groups at −4 ppm. Similarly, integration of the silicon peak corresponding to the Si–O–Si backbone at −21 ppm gave the number of dimethylsiloxy units, N_D. Owing to the presence of one vinyl group for each end group, N_{vin} must be divided by 2 and then compared with the integrated area due to the dimethylsiloxane units N_D of the polymer. Based upon this analysis, it was found that the synthesized PDMS has a degree of polymerization of 1225 and that its M_n is ∼90,827. The molecular weight of the polymer did not change, when polymerization was carried out in presence of filler.

3.2. Characterization of the nanocomposites

3.2.1. WAXD studies in low angle range

The X-ray diffractograms of the sepiolite clay and in situ PDMS-sepiolite nanocomposites are shown in Fig. 4. The clay shows a peak in the range of 7.2–7.4° (2θ), corresponding to the d-spacing of 1.22–1.24 nm. In contrast, dispersed hybrids exhibit no distinct features in this 2θ range. In the present case, lack of a definite diffraction pattern in the hybrid is an evidence for high degree of dispersion of sepiolite in the matrix. This is in well accordance with the observation made by Benlikaya et al. [33]. Unlike MMT [34], where individual tetrahedral and octahedral layers can easily be separated, sepiolite exhibits a structure where individual TOT (tetrahedral octahedral tetrahedral) layers are strongly bonded. Unlike smectite clays, here fiber bundles or aggregates get separated into nanometer dimension when these fillers are dispersed into the polymer matrix. Good dispersion of the clay refers to complete isolation of the individual fibers from each other. As shown in the figure, disappearance of the 110 peak of sepiolite in XRD patterns of nanocomposites is considered as an evidence for good dispersion of the sepiolite fibers. In fact, as shown in the TEM images later individual fibers with 10–12 nm, especially for lower loadings, are well dispersed in the matrix. However, small XRD peak is observed for the nanocomposites with higher loadings, which is due to agglomeration of the filler. Intensity of the 110 peak is related to the volume fraction of sepiolite fibers, i.e., lower the volume fraction of fibers, weaker the diffraction peak [33]. These observations are different from those reported in our earlier communications where sepiolite-HNBR nanocomposites exhibit a strong XRD pattern around 7° even at lower concentrations [18]. This may be the effect of in situ polymerization inside the silicate layers which pushes apart the individual fibers of the clay. In the earlier studies on HNBR, however, the composites were formed ex situ. In spite of our best efforts by various techniques and solvents, the layers in sepiolite could not be separated earlier. But in the case

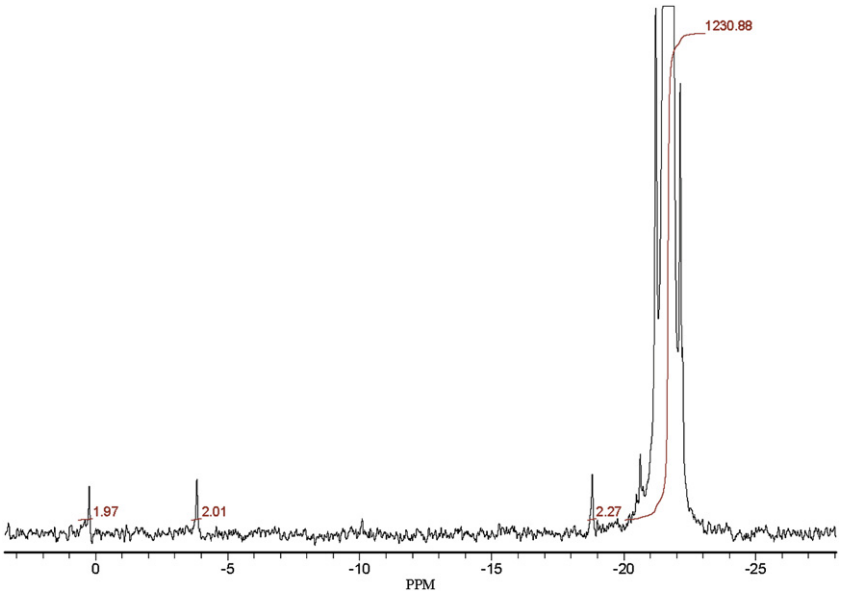

Fig. 3. ^{29}Si NMR spectrum of synthesized vinyl terminated PDMS.

of in situ synthesis of nanocomposites, greater extent of dispersion is achieved.

3.2.2. TEM studies

TEM observations reveal that a complete disagglomeration of the fibrous cluster of the sepiolite filler is achieved in the nanocomposites. Fig. 5 shows the bright field TEM images of 2, 4, 6 and 8 phr sepiolite loaded in situ nanocomposites and 4 phr sepiolite loaded ex situ nanocomposite. The bright background shows the polymer matrix while the dark rod-like structures are individual fibers of sepiolite. Fibrous nature of sepiolite is confirmed from the TEM images. The diameter of a single fiber is observed to be around 10–12 nm, while approximate diameter of the fiber bundles in sepiolite is approximately 100–350 nm. In Fig. 5a (2 phr loading), individual fibers are well dispersed and separated from each other. Thus finest extent of dispersion is achieved. Even in Fig. 5b and c (4 phr and 6 phr loadings) the samples exhibit high quality dispersion. Indeed, presence of individual needles can be observed without any remaining bundle-like aggregate. Fig. 6a is a high resolution TEM image for 4 phr filler loaded in situ nanocomposites. For more precision in the study, image analysis was done using image J software. Background correction for uniform illumination and conversion to threshold image gave the image shown in Fig. 6b which shows the fillers much more prominently for estimation of the diameter and hence interpreting the degree of dispersion. Conversion of the distance in pixels into distance in nanometer helps in determining the thickness of each individual fiber which was found to be 10 ± 2 nm. This is, in fact, the thickness of individual fibers of sepiolite [19]. In situ polymerization in presence of fillers is probably more effective in causing better disagglomeration of the sepiolite bundles. Detailed study of sepiolite structure reveals that there are narrow channels in between the TOT layers [18]. During the formation of in situ nanocomposites, monomer molecules preferentially enter into these channels, where they undergo polymerization, thereby accounting for complete disruption of the agglomerated structure. At higher loadings, however, agglomeration of the filler takes place, which is observed in Fig. 5d. For better comparison, TEM image for ex situ prepared nanocomposites with 4 phr sepiolite loading is shown in Fig. 5e. Here, agglomerates are much more prominent compared to individually dispersed fibers. This suggests the advantage of in situ synthesis of nanocomposites over those prepared by ex situ method. This is manifested in the greater improvement in mechanical and thermal properties which is discussed in the subsequent sections.

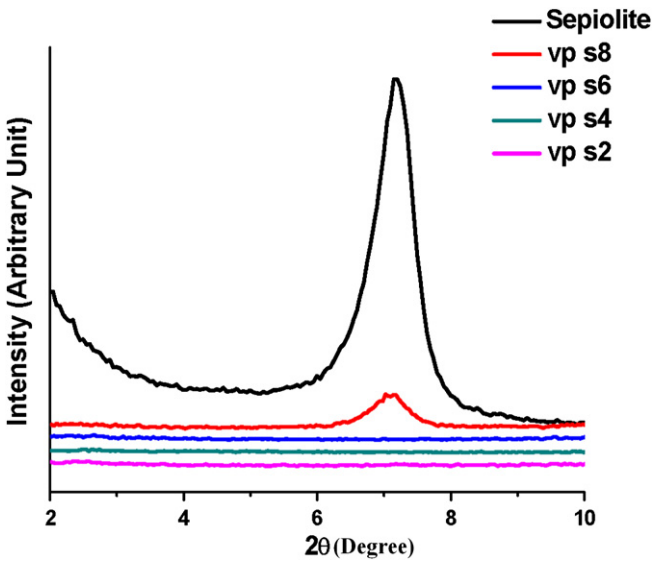

Fig. 4. Comparison of the WAXD plots (in low angle range) of sepiolite and various sepiolite loaded samples.

Determination of aspect ratio of nanofiller

In order to determine the aspect ratio of reinforcing filler in the nanocomposite, image analysis has been done with the TEM images of 4 phr (Fig. 5b) and 6 phr (Fig. 5c) sepiolite loaded samples. In general, larger area is scanned in comparison to those shown in the above mentioned figures. The length and thickness of individual particles are determined as mentioned earlier by image analysis and thereby aspect ratio is calculated using equation (3).

$$\text{Aspect ratio of filler}(\alpha) = \frac{l}{t} \tag{3}$$

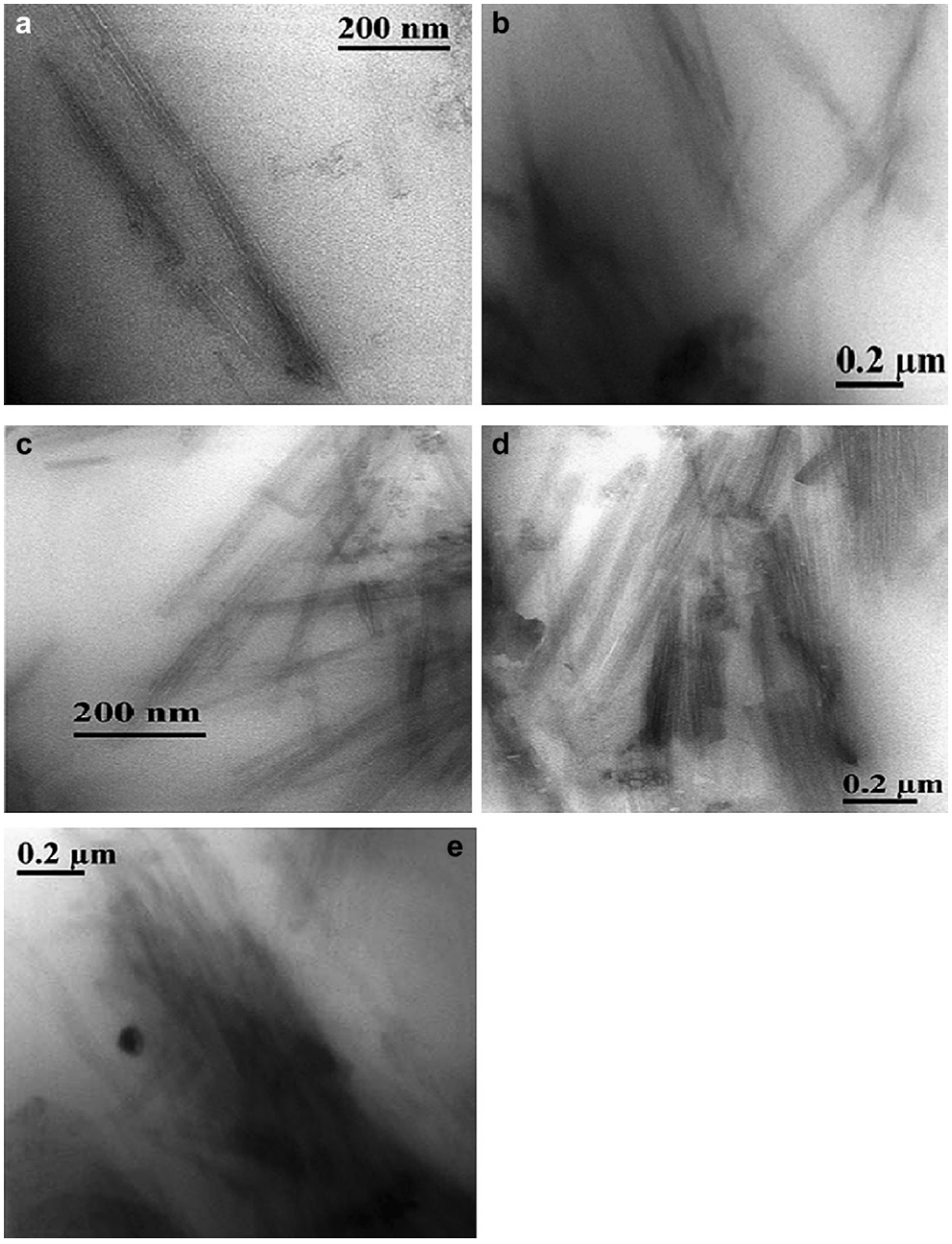

Fig. 5. TEM images of a) 2 phr, b) 4 phr, c) 6 phr and d) 8 phr sepiolite loaded in situ nanocomposite e) 4 phr sepiolite loaded ex situ nanocomposite.

where l is the particle length and t is the thickness of the particle. These two figures are chosen for image analysis since dispersion of the filler is better in these specimens resulting in more precise results. The data corresponding to the calculation of aspect ratio of filler is converted into histogram (Fig. 7) for statistical analysis. From the histogram the average aspect ratio of the sepiolite filler is found to be 31. These data has been used in the subsequent sections in order to model the modulus of rubber-clay nanocomposites.

3.2.3. ATR-FTIR studies

The FTIR spectra of pristine PDMS and sepiolite based nanocomposites give evidences for the interaction between the polymer and the fibrous silicate layers as shown in Fig. 8. The characteristic peaks of vinyl terminated PDMS are as follows: prominent peaks are found at 2964 cm^{-1} for asymmetric CH stretch, 1408 cm^{-1} due to CH_3 asymmetric deformation, 1259 cm^{-1} CH_3 symmetric deformation, Si–O–Si asymmetric deformation around 1030 cm^{-1}, Si–O–Si skeletal stretching around 800 cm^{-1} and 695 cm^{-1} for the surface [35].

Shift in the absorptions for Si–O–Si asymmetric deformation and Si–O–Si skeletal deformation are less vivid for lower loadings but is well observable when the filler content is considerably increased (sample with 20 phr loading). The peak for Si–O–Si asymmetric deformation shifts from 1039 cm^{-1} for virgin PDMS to 1013 cm^{-1} for 20 phr sepiolite loaded sample and the peak for Si–O–Si skeletal stretching shifts from 815 cm^{-1} to 782 cm^{-1} for 20 phr sepiolite loaded sample. Increase in intensity of the peak at 3500 cm^{-1}, which is due to OH stretching of the H-bonded silanol groups, is observed for the nanocomposites (even with lower loadings). This peak is altogether absent in neat PDMS, and the

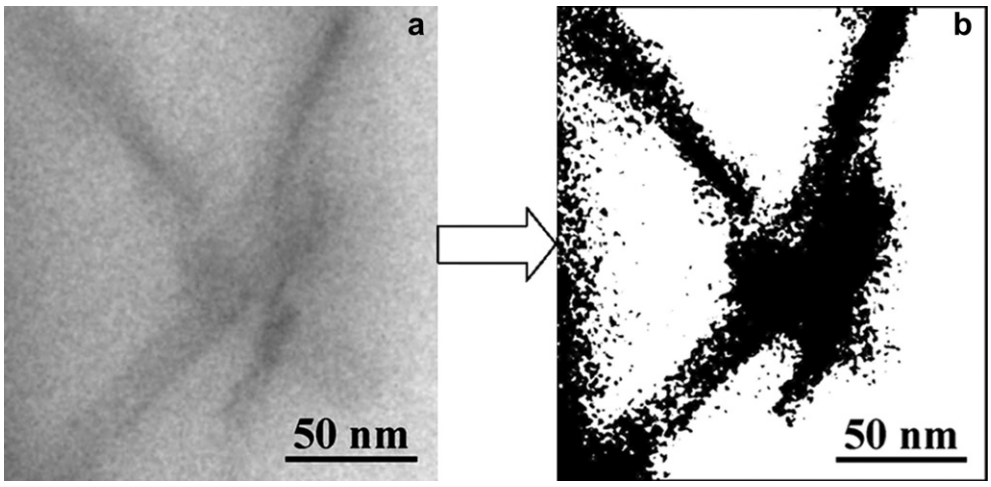

Fig. 6. High resolution TEM image of a) 4 phr sepiolite loaded nanocomposite b) 4 phr sepiolite loaded nanocomposite subjected to image analysis (background correction then conversion to threshold image).

intensity increases with increase in the filler loading. When compared with the absorption peak for OH group of sepiolite, the peak for the nanocomposites is found to show a prominent shift, thereby showing interaction of filler with PDMS backbone. However, intensity of OH absorption is much more in the case of sepiolite compared to those of the nanocomposites due to very small amount of the filler in the polymer matrix. It is clearly understandable that the peak shift of OH absorption is towards lower frequency [36]. This is most probably due to weakening of the OH bond as a result of H-bonding.

3.2.4. WAXD studies in high angle range

WAXD was carried out for the virgin elastomer and the nanocomposites to determine the restriction process of crystallization in the nanocomposites as a function of the amount of sepiolite incorporated. Fig. 9 illustrates the WAXD spectra of the samples. In the figure, the neat polymer exhibits a sharp reflection at 2θ of 12.54° and a broad reflection at 22.74° corresponding to the centered tetragonal unit cell, which is in accordance with earlier research [37]. When polymerization is carried in presence of 2 phr of sepiolite, it gives a slightly broader reflection at 12.34°. The

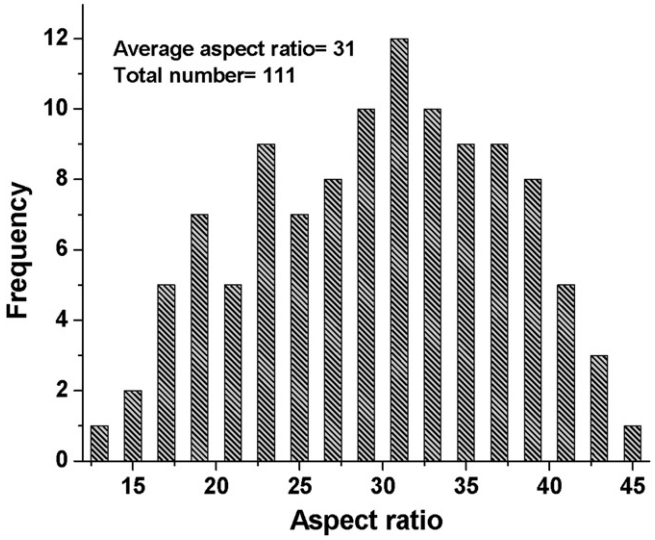

Fig. 7. Histogram of sepiolite aspect ratio obtained from image analysis of representative sample.

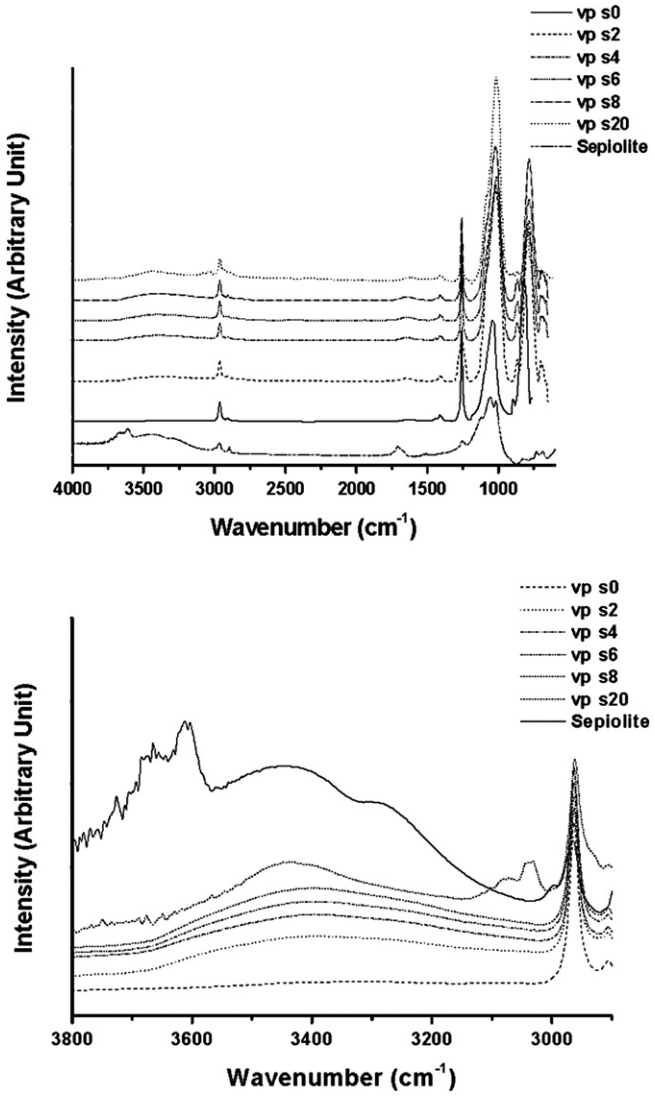

Fig. 8. Comparison of the FTIR plots of unfilled, sepiolite-filled PDMS systems and sepiolite.

broader reflection at 22.74° also undergoes slight flattening in the case of 2 phr loaded sample. As percentage of sepiolite goes on increasing, intensity of reflection at 12.54° and 22.74° goes on decreasing. Further, there is a gradual shift in position of the reflection at 12.54° towards lower value of 2θ. These results suggest that incorporation of increasing amount of filler during polymerization hinders the crystalline domain formation and thereby decreases the size of the growing crystallites. This is in well agreement with the results obtained from DMA discussed later. With progressive increase in filler amount, the PDMS peak is shifted slightly. Although the crystallinity is affected, no new reflection appears, indicating that no new packing structure or unit cell is formed. The reduction in crystallite size demonstrates a gradual decrease in orderness in the crystal phase, reflecting phenomena such as dislocations, point defects, etc., generated among the crystalline grains [37].

The molecular chains of PDMS possess a regular helical conformation [38] and the highly symmetric crystallite of PDMS belongs to the centered tetrahedron system. WAXD studies reveal that there is no change in crystalline packing in the nanocomposites. When polymerization occurs in the narrow channels of sepiolite, the growing polymer chains interact with the silanol groups of filler and thereby are forced to attain a conformation which is different from its conformation in the native state necessary to generate the crystallites. This, probably, is the reason for reduction in intensity of reflection and peak shift.

The d values were calculated using equation (1) and crystallite size was estimated by using equation (2) and the values are depicted in Table 2. There is a prominent shift in position of the diffraction peak around 12°. The peak appears at a 2θ value of 12.54° for neat polymer (vp s0) but shifts to 12.13° for vp s10. This suggests a decrease in size of the crystalline domains which has been calculated to be 1.38 nm. The full width at half maxima (FWHM) is found to increase from 2.08° for vp s0 to 2.86° for vp s10 suggesting peak broadening which is the consequence of imperfect crystallite formation.

3.2.5. Dynamic mechanical analysis

Dynamic mechanical analysis has been widely used in rubber nanocomposite systems in order to investigate polymer chain dynamics. Figs. 10 and 11 illustrate plots of tanδ and storage modulus as a function of temperature. The values of tanδ are shown in Table 3. The plot of tanδ versus temperature of the neat PDMS shows three prominent peaks or transitions at −117 °C, −57 °C and −29 °C. The first transition corresponds to the segmental relaxation associated with the glass transition of the amorphous phase of PDMS [39]. The peak for the relaxation corresponding to glass transition temperature (T_g) appears at approximately same position in the temperature axis for the nanocomposites. However, there is a decrease in the height of the tanδ peak corresponding to T_g which is due to polymer-filler interaction [40]. Mathematical interpretation has been offered by Fornes and Paul. Low values for tanδ are simply because of dividing the almost constant loss modulus values by the larger storage modulus values [41]. The peak at −57 °C is due to the crystalline peak which is due to the presence of microcrystallites, which has already been depicted in the WAXD studies and that at −29 °C is due to melting of the crystallites [9]. The peak at −57 °C is due to formation of the crystalline domains once the T_g is crossed [42]. The melting peak is much more prominent than the crystallization peak owing to greater mobility of the PDMS chains that make a three-dimensional chain arrangement necessary for crystalline phase development [39]. There is a drastic decrease in the height of the former peak which is rather converted to a broad hump spanning a region of 100 °C. This is probably due to loss in crystallinity of the polymer in presence of filler [43].

Analysis of viscoelastic properties of the samples exhibits some sort of similarities. Unfilled PDMS as well as the nanocomposites exhibit a glassy region below −117 °C with the magnitude of storage modulus exceeding 10^3 MPa. For virgin polymer a three-step descent is generally observed. First two descends correspond to the decrease in modulus due to transition from glassy state to

Table 2
Determination of d-spacing for the reflection at 110 plane and crystallite size.

Sample	2θ (°)	d-spacing (nm)	Assignment	[a]FWHM (°)	Crystallite size (nm) (110)
vp s0	12.54	0.706	110	2.08	1.92
vp s2	12.34	0.719	110	2.46	1.62
vp s4	12.26	0.722	110	2.61	1.53
vp s6	12.20	0.725	110	2.72	1.47
vp s8	12.20	0.725	110	2.73	1.46
vp s10	12.13	0.729	110	2.86	1.38

[a] FWHM is full width at half maxima.

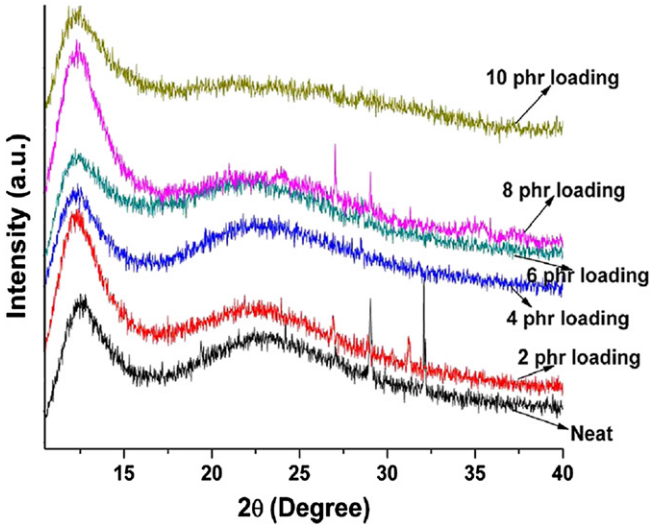

Fig. 9. Comparison of the WAXD plots of the unfilled and the sepiolite-filled PDMS systems.

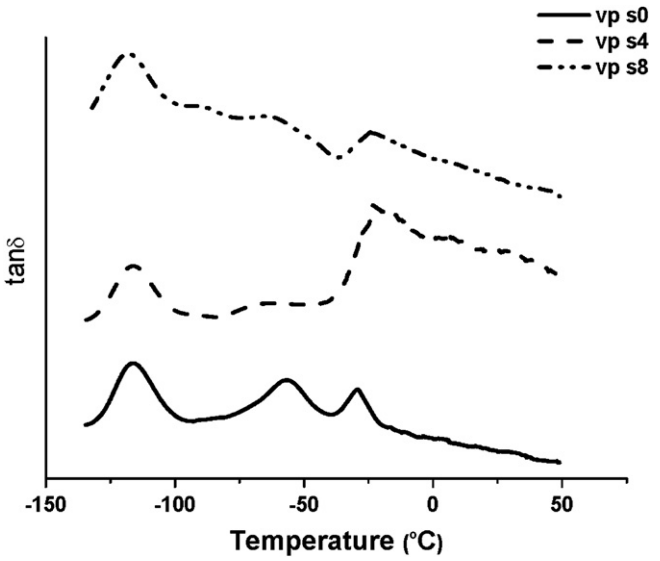

Fig. 10. Comparison of tan δ of the neat PDMS and sepiolite loaded samples.

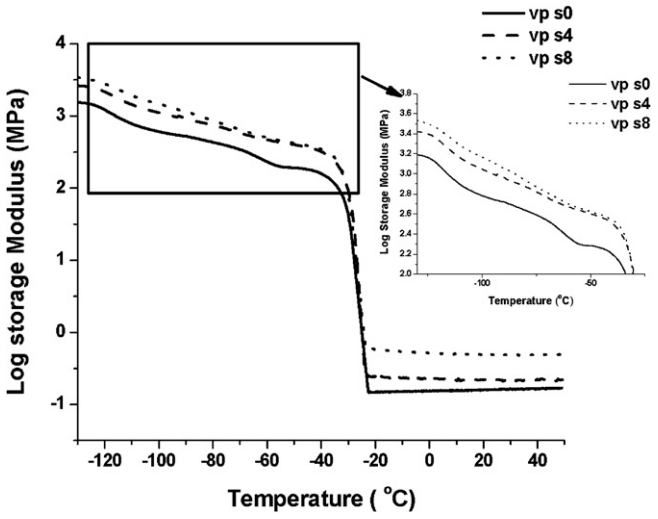

Fig. 11. Comparison of storage modulus of the neat PDMS and sepiolite loaded samples.

rubbery state and the crystallization phenomenon thereby suggesting that a greater amount of storage modulus is due to the crystallites [39]. The small drop in E′ in the glass transition region is due to the presence of crystalline domains in PDMS. These domains behave in the similar way as crosslinks, thereby reducing the E′ fall [44]. This is followed by an abrupt descent until a plateau is characterized by a specific modulus value for each sample, thereby marking the phenomenon of melting of crystalline phase of the polymer. The variation in E′ with temperature attains a constant level beyond −20 °C up to 150 °C, in spite of quite low magnitude of E′, characteristic of the conventional elastomer. E′ at 25 °C is found to increase with increase in filler loading. It increases from 0.164 MPa to 0.232 MPa for 2 phr of filler loading, while it shows a 200% increase and attains a magnitude of 0.503 MPa for 8 phr filler loading. The effect of the polymer-filler interaction manifests more in the magnitude of E′ at 25 °C than in the glassy region. This is due to the fact that above T_g the material becomes soft and reinforcement of the filler becomes more prominent due to restricted motion of the macromolecular chains [40].

Storage modulus increases with increase in crystalline domains in the matrix as observed by Modesti et al. [45]. Thus decrease in crystalline domain decreases modulus of the material. In fact, storage modulus of the nanocomposites depends on the two opposing factors: increase in polymer-filler interaction and decrease in the crystalline phase. For lower loadings of the filler the two effects almost nullify each other, thereby reducing the difference in E′ between the neat PDMS and the nanocomposites. But with increase in the filler loading, the former of the two opposing effect takes the upper hand and the E′ increases, though the increase in E′ is less pronounced. Another point which needs to be discussed is that the second descent decreases in magnitude due to the decrease in crystalline phase in the nanocomposites as is evident from WAXD studies.

Table 3
Determination of tan δ values of virgin PDMS and its sepiolite based nanocomposites.

Sample Designation	tan δ	E′ at 25 °C (MPa)
vp s0	0.195	0.164
vp s4	0.121	0.232
vp s8	0.107	0.503
VP S8	0.131	0.399

Decrease in tanδ height corresponding to T_g and E′ at 25 °C for ex situ nanocomposites suggests reduced polymer-filler interaction compared to in situ nanocomposites. This is probably due to agglomeration of filler as observed from the TEM image.

3.2.6. Mechanical properties

Mechanical properties of the PDMS-sepiolite nanocomposites are enlisted in Table 4. The representative stress–strain plots of the samples are shown in Fig. 12 and comparison of tensile strength and modulus at 100% elongation at various filler loadings in the nanocomposites are shown in Fig. 13. It is found that tensile strength increases by 90%, 153%, 200%, 209% and 211% for 2, 4, 6, 8 and 10 phr loadings of the fillers. Increase in tensile strength for 4–6 phr filler loading is much more (47%) compared to that for 6–8 phr (9%) or for 8–10 phr loading (2%). Thus saturation in the increase in tensile strength occurs for 6 phr filler loading. Modulus at 100% elongation for these same filler loadings are respectively 134, 213, 240, 246 and 350 kPa, while that of the unfilled PDMS is 62 kPa. Hence, there is a significant increase in the magnitude of modulus at 100% elongation for the nanocomposites as compared to the unfilled vulcanizate. But nanocomposites with higher loadings of the filler do not show any remarkable improvement in the modulus value. Polymer-filler interaction increases tensile strength and modulus for the nanocomposites [46]. On the other hand, decrease in size of the crystalline domains reduces tensile strength and modulus [47]. The results obtained here are due to complication of the situation by the simultaneous role played by the opposing factors, namely the polymer-filler interaction, intercalation versus aggregation phenomena and the loss in the crystalline phase development in the nanocomposites. However, polymer-filler interaction, which is a direct function of exfoliation, has a greater impact in determining the mechanical properties making the loss in crystalline domain recessive in contributing towards tensile properties and modulus values. It shows its prominent effect in determining the magnitude of modulus at 100% elongation. As the amount of filler increases, the orientation necessary for PDMS chains to attain the crystalline domain is restricted. The crystalline domain has an important role to play in determining the modulus, as has been observed from the results of DMA. Polymer-filler interaction has a more prominent role to play and hence a smooth increase in the modulus at 100% elongation is observed for the nanocomposites at higher loadings. Elongation at break (EAB) decreases in the case of the nanocomposites as compared to the unfilled elastomer but a rather irregular pattern is observed with increasing loading of sepiolite. Decrease in EAB for the nanocomposites is due to restriction imposed on the polymer chains by the surface functional groups of sepiolite [48].

For the ex situ prepared nanocomposites, tensile strength increment is 117% and 143% for 4 and 8 phr filler loadings respectively, while for in situ nanocomposites it was comparatively much more as mentioned earlier. Even modulus at 100% elongation increment shows similar trend. It is just 154% and 198% for VP S4

Table 4
Comparison of the mechanical properties of the nanocomposites.

Sample Designation	E_{mod} (kPa)	Tensile Strength TS (kPa)	Modulus at 100% Elongation (kPa)	Elongation at break EAB (%)
vp s0	140 ± 20	167 ± 12	62 ± 10	506 ± 59
vp s2	225 ± 31	324 ± 30	134 ± 3	388 ± 8
vp s4	345 ± 65	429 ± 22	213 ± 4	234 ± 15
vp s6	445 ± 39	508 ± 15	240 ± 13	247 ± 4
vp s8	488 ± 48	526 ± 32	246 ± 7	285 ± 8
vp s10	516 ± 19	529 ± 41	350 ± 14	184 ± 13
VP S4	328 ± 12	363 ± 13	158 ± 6	332 ± 4
VP S8	341 ± 20	406 ± 21	185 ± 11	206 ± 9

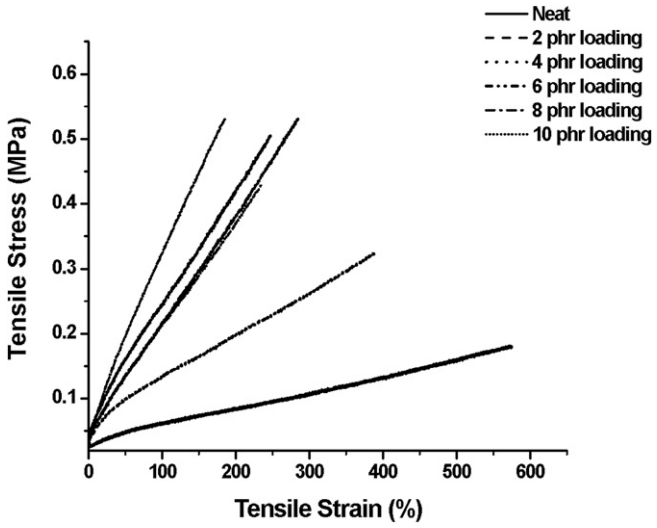

Fig. 12. Comparison of stress–strain curves for the unfilled and the filled samples.

and VP S8. This shows that in situ nanocomposites impart better polymer-filler interaction probably due to greater interfacial adhesion.

To get a clear picture of the filler reinforcement, experimental data of the tensile modulus were compared with the authentic models relating tensile modulus as a function of filler volume fraction. Guth and Gold equation [49] explained the reinforcing effect of colloidal filler particle by introducing a quadratic term on the basis of Smallwood–Einstein equation which takes into account the interaction between the filler particles. The equation given by them is as follows:

$$E = E_m\left[1 + 2.5\phi + 14.1\phi^2\right] \tag{4}$$

where E and E_m are the Young's modulus of the nanocomposite and matrix respectively and ϕ is the volume fraction of filler. However, equation (4) is applicable only to spherical particulates filled composites.

The above equation was modified by Guth [50] by introducing a factor α (length/thickness), also known as "aspect ratio" of the filler, into the above equation to consider the effect of accelerated stiffening.

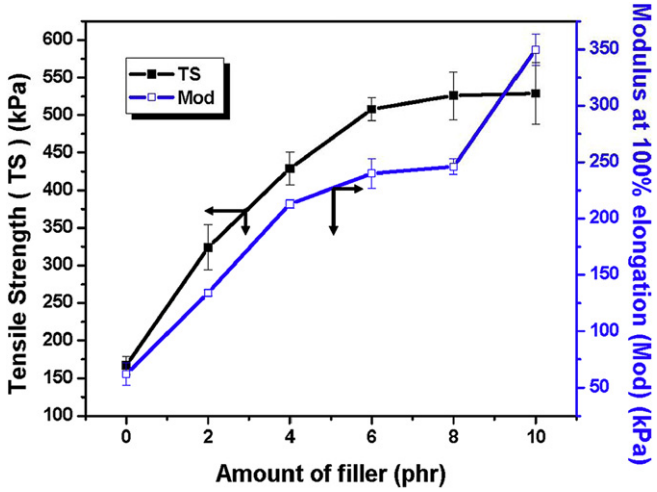

Fig. 13. Plots of tensile strength and modulus at 100% elongation at various loadings of the filler.

$$E = E_m\left[1 + 0.67\alpha\phi + 1.62(\alpha\phi)^2\right] \tag{5}$$

The magnitude of E is found to show a sharp increase with increasing filler volume fraction as is evident from Fig. 14. Thus Guth equation has been chosen as the model for our study. Halpin-Tsai equation [51–53] also serves as a model in this case since it is accurately used to estimate the reinforcement effects of filler in the nanocomposites. The elastic modulus of the nanocomposites filled with fibrous reinforcing particulates is expressed by Halpin-Tsai as follows:

$$\frac{E}{E_m} = \frac{(1 + \xi\eta\phi)}{(1 - \eta\phi)} \tag{6}$$

In Eq. (6), ξ depends upon geometry and orientation of the filler and also on loading direction. The term η is expressed as

$$\eta = \frac{\frac{E_f}{E_m} - 1}{\frac{E_f}{E_m} + \xi} \tag{7}$$

where E_f is the Young's modulus of filler.

$$\text{Moreover, } \xi = 2\alpha \tag{8}$$

Fig. 14 compares the experimental modulus data with the model predictions taking into consideration the value of α as determined from the TEM image analysis. It is found that experimental data agree well with the Guth and Halpin-Tsai model for low filler volume fraction (upto 6 phr filler loading). With further increase in filler loading the modulus of the nanocomposite is found to show a decrease in magnitude compared to the models. The probable reason for this is the decrease in modulus of the matrix phase in the nanocomposites due to loss in crystalline domain. Ex situ nanocomposites show even much lower modulus value with increasing filler loading which is probably due to agglomeration of filler as is evident from the TEM image.

3.2.7. Thermogravimetric analysis

The improvement in the thermal degradability of the nanocomposites in comparison to the virgin polymer is shown in Figs. 15 and 16 which are respectively the TGA and DTG plots of the unfilled

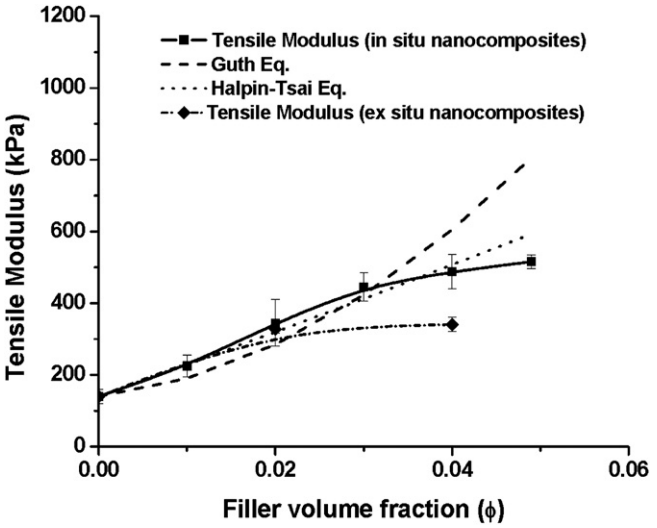

Fig. 14. Experimentally determined tensile modulus and theoretical predictions by Guth and Halpin-Tsai model.

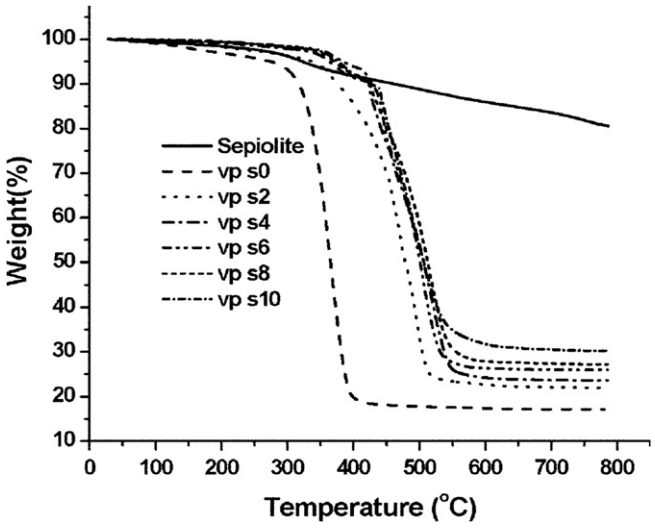

Fig. 15. Comparison of the TGA curves of the unfilled, filled PDMS and sepiolite.

PDMS and the nanocomposites containing 2, 4, 6, 8 and 10 phr of sepiolite. Inclusion of a nanoscale dispersion of the sepiolite into the in situ generated PDMS matrix leads to an increase in the overall oxidative thermal stability of the elastomeric matrix.

For the unfilled polymer, there is a single degradation temperature at 350 °C. Detailed study of the thermal degradative behavior made by Lewicki et al. by thermal volatilization analysis suggests that several cyclic volatile oligomeric siloxanes, primarily D_3, D_4 and D_5 are formed during thermal degradation of the polymer, D_3 being the major volatile product [54]. However, the end product of oxidative thermal degradation of PDMS is silica as has been reported by Camino et al. [55]. Hence, residue is obtained in the TGA trace for the virgin elastomer. The TGA curves of the nanocomposites follow an altogether different trend as compared to the neat PDMS. Sepiolite, in fact, plays a dominant role in the enhancement of thermal stability of the nanocomposites [56]. Comparison of the DTG plots of the nanocomposites with that of the sepiolite helps in rather understanding the mechanism of the role played by the filler in imparting thermal stability to the polymer matrix in the nanocomposites. While the DTG plot of the virgin polymer shows only one hump, those of the nanocomposites show one small broad hump followed by a big sharper hump. The position of this latter hump helps in determining the T_{max} of the nanocomposites which gives a vivid idea regarding the thermal stability improvement in the case of the nanocomposites. The values of the T_{max} are depicted in Table 5. Sepiolite has only one prominent hump in the DTG curve around 350 °C which is, in fact, observed in the DTG curves of the nanocomposites. This clearly suggests that due to prominent interaction between the filler and the polymer chains, the latter enter into the nano-dimensioned channels and are held there by the H-bonding interaction with the silanol group. In between 300 and 400 °C major decomposition reaction is degradation of the organic quaternary ammonium ions to liberate several volatile products such as CO, CO_2, water, HCl and NH_3. The higher T_{max} and increased amount of char residue are mainly due to the fact that heat conduction into the polymer matrix is retarded by the well dispersed fibrous silicate layers since

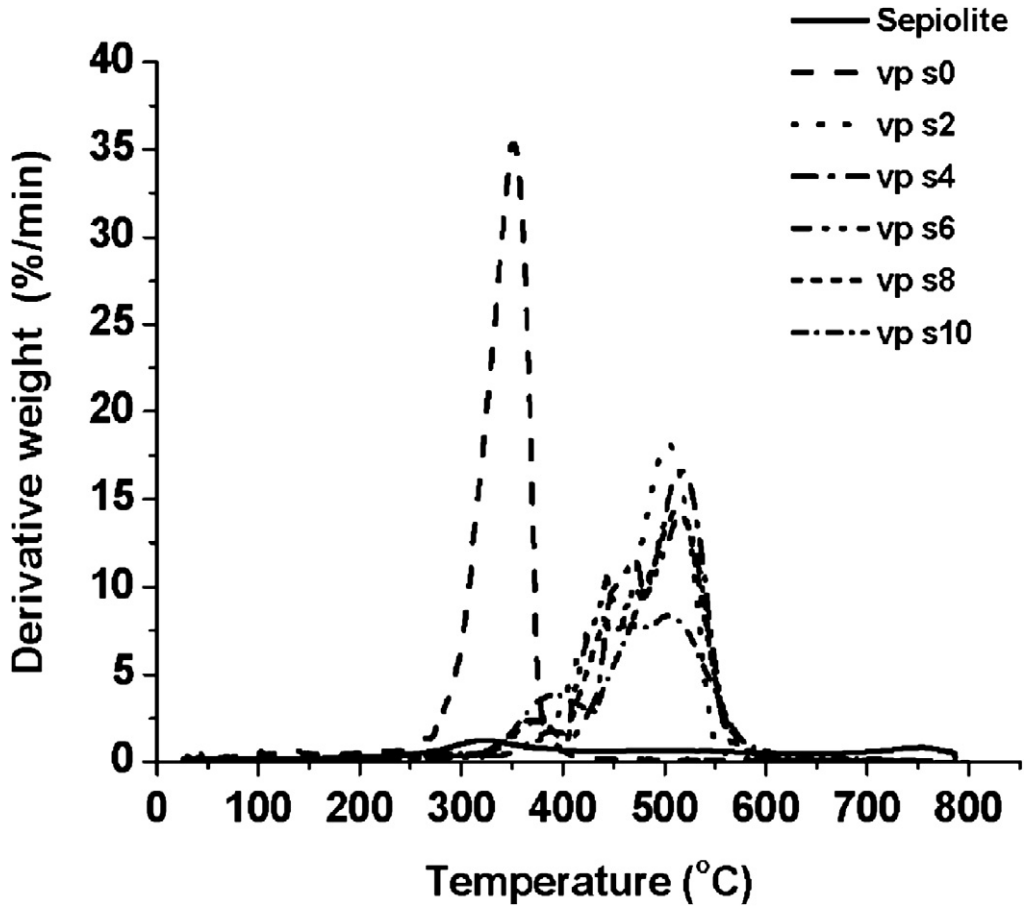

Fig. 16. DTG curves of the unfilled and sepiolite-filled PDMS.

Table 5
Comparison of T_{max} and T_i of the neat PDMS and nanocomposites.

Sample	T_{max} (°C)	T_i (°C)	Ash content (%)	Rate of Degradation (%/min)
vp s0	350	332	18.25	35.34
vp s2	503	430	21.87	18.24
vp s4	516	437	23.69	16.71
vp s6	517	450	25.92	13.95
vp s8	512	443	27.46	14.36
vp s10	502	409	30.50	8.41
VP S4	441	373	22.76	16.93
VP S8	496	425	26.70	16.80

sepiolite restricts mobility of the polymer chains [56]. Sepiolite acts as the mass transport barrier to the volatiles produced during decomposition. Unlike MMT, the needle-like structure of sepiolite increases tortuosity of diffusion pathways, thus delaying loss in the volatiles. Physi- and/or chemi-sorption occurring at the filler-matrix interphase may lead to formation of physical network thereby enhancing the nanocomposite stability [56,57]. Comparison of the thermal stability of the nanocomposites at various loadings suggests that both the temperature of maximum degradation T_{max} and the temperature of onset of degradation T_i increase upto 6 phr loading of filler, but for higher loadings these decrease gradually due to agglomeration of the filler. These values are, however, much higher than those of the virgin elastomer. Even the rate of degradation significantly decreases with increase in filler content which is due to the reasons mentioned above.

Ex situ prepared nanocomposites show increased oxidative thermal stability but to a much lesser extent as compared to the in situ nanocomposites with similar filler loading. The probable cause may be as follows: since in the case of in situ nanocomposites the monomers enter into the narrow channels of the filler and thereafter polymerization takes place, there is a greater interfacial area for interaction available for the polymer and the filler compared to the ex situ nanocomposites. Table 5 is a compilation of the data related to the thermogravimetric analysis.

4. Conclusions

PDMS-Sepiolite nanocomposites have been synthesized by anionic ring opening polymerization of octamethylcyclotetrasiloxane (D_4). Nanocomposites have been prepared with higher loadings of the filler and cured using platinum catalyst and a crosslinker having Si–H functionality. Then, a detailed analysis of structure-property relationship has been carried out.

Sepiolite has been found to interact with the polymer matrix through H-bonding with the main polymer skeletal chain. High degree of dispersion of filler has been observed from image analysis of the TEM images of the nanocomposites. Thickness of the individual fibers has been found to be 10–12 nm and the average aspect ratio of the fibers is 31. Good interaction between the filler and the polymer matrix occurs as polymerization takes place in the presence of filler. This leads to improvement in thermal, dynamic and static mechanical properties of the polymer. Thermal properties enhancement is observable by the huge improvement in T_{max} and T_i. Mechanical properties enhancement is, in fact, vivid from the increased values of tensile strength and modulus at 100% elongation for the nanocomposites as compared to those of the unfilled elastomer. Tensile strength has been found to increase by 210% for 10 phr loading of sepiolite, while the modulus at 100% elongation undergoes an increment of 460% for the same filler loading. However, ex situ prepared nanocomposites show lower improvement in tensile strength and modulus compared to in situ synthesized nanocomposites. Halpin-Tsai and Guth model has been used to predict the modulus of rubber-clay nanocomposites for low filler loading. Deviation from the models is observed for high filler loading due to agglomeration of filler and decrease in crystalline domain size. DMA results show improvement in storage modulus, thereby explaining the phenomenon of polymer-filler interaction. FTIR spectra of the nanocomposites when compared with those of the neat PDMS and sepiolite indicate interaction between the components. However, WAXD studies show a decrease in the crystallite domain in PDMS matrix during nanocomposite synthesis. The result is, obviously, decrease in mechanical properties of the polymer system, as these crystallites act as crosslinks providing strength to the matrix. But this factor is negated by the even more prominent polymer-filler interaction which improves the properties of the nanocomposites. Good dispersion of the filler in the polymer matrix as observed from the WAXD and TEM studies yields improved mechanical and thermal properties.

Acknowledgement

The financial grant for this work by Council of Scientific and Industrial Research (CSIR), New Delhi to Mr. Nabarun Roy is gratefully acknowledged. Professor Anil K. Bhowmick is grateful to Indo-Australia Strategic Research Fund, Department of Science and Technology, New Delhi for supporting a programme on polymer nanocomposites.

References

[1] Sun CC, Mark JE. Polymer 1989;30:104–6.
[2] Jose-Yacaman M, Rendon L, Arenas J, Puche MCS. Science 1996;273:223–5.
[3] McCarthy DW, Mark JE, Clarson SJ, Schaefer DW. J Polym Sci Part B Polym Phys 1998;36:1191–200.
[4] Landry CJT, Coltrain BK, Landry MR, Fitzgerald JJ, Long VK. Macromolecules 1993;26:3702–12.
[5] Rajan GS, Sur GS, Mark JE, Scaefer DW, Beaucage G. J Polym Sci Part B Polym Phys 2006;41:1897–901.
[6] Dewimille l, Bresson B, Bokobza l. Polymer 2005;46:4135–43.
[7] Xu J, Razeeb KM, Roy S. J Polym Sci Part B Polym Phys 2008;46:1845–52.
[8] Wang J, Chen Y. J Appl Polym Sci 2006;107:2059–66.
[9] Burnside SD, Giannelis EP. J Polym Sci Part B Polym Phys 2000;38:1595–604.
[10] Chen B, Zhan X, Yi L, Chen F. Chin J Chem Eng 2007;15:661–5.
[11] Bhattacharya M, Bhowmick AK. Polymer 2008;49:4808–18.
[12] Maji PK, Das NK, Bhowmick AK. Polymer 2010;51:1100–10.
[13] Ganguly A, Bhowmick AK. Macromolecules 2008;41:6246–53.
[14] Sadhu SD, Rajeev RS, Bhowmick AK. Polym Polym Compos 2008;16:283–93.
[15] Datta H, Singha NK, Bhowmick AK. J Appl Polym Sci 2008;108:2398–407.
[16] Ray SS, Okamoto M. Prog Polym Sci 2003;28:1539–641.
[17] Preschilla N, Sivalingam G, Rasheed ASA, Tyagi S, Biswas A, Bellare JR. Polymer 2008;49:4285–97.
[18] Choudhury A, Bhowmick AK, Ong C. Polymer 2009;50:201–10.
[19] Ma J, Bilotti E, Peijs T, Darr JA. Eur Polym J 2007;43:4931–9.
[20] Duquesne E, Moins S, Alexandre M, Dubois P. Macromol Chem Phys 2007;208(23):2542–50.
[21] Xie S, Zhang S, Wang F, Yang M, Séguéla R, Lefebre MJ. Compos Sci Technol 2007;67:2334–41.
[22] Darder M, Lopez-Blanco M, Aranda P, Aznar AJ, Bravo J, Ruiz-Hitzky E. Chem Mater 2006;18:1602–10.
[23] Bokobza L, Burr A, Garnaud G, Perrin MY, Pagnotta S. Polym Int 2006;53:1060–5.
[24] Santiago F, Micientes AE, Osorio M, Poblete FJ. Polym Int 2006;55:843–8.
[25] Zheng Y, Zheng Y. J Appl Polym Sci 2006;99:2163–6.
[26] Ma J, Bilotti E, Peijs T, Darr JA. Eur Polym J 2007;43(12):4931–9.
[27] Deneubourg FX, Beigbeder A, Degée Ph, Viville P, Dubois Ph. Silicone-based nanocomposites: new materials for antifouling coatings. Available at, http://morris.umh.ac. be/SMPC/Posters/2006-BPG-FRDE.pdf.
[28] Bokobza L. J Appl Polym Sci 2004;93:2095–104.
[29] Mo ZS, Zhang HF. Structure of crystalline polymer and x-ray diffraction [M]. Science Press: PRC; 2003. p. 232.
[30] Pawlenko S. Organosilicon chemistry. Berlin, Germany: Walter de Gruyter & Co.; 1986.
[31] Chalk AJ, Harrod JF. J Am Chem Soc 1965;87:16–21.
[32] Urman YG, Alekseyeva SG, Amerik VV, Balabushevich AG, Arshava BM, Slonim IYa, et al. Polym Sci U.S.S.R 1980;22:1027–37.
[33] Benlikaya R, Alkan M, Kaya İ. Polym Composite 2009;30:1585–94.
[34] Maiti M, Bhowmick AK. J Polym Sci Part B Polym Phys 2006;44(1):162–76.
[35] Socrates G. Infrared characteristic group frequencies. Bristol: John Wiley and Sons; 1980 [Chapter 18], p. 126–127.
[36] Li D, Brisson J. Polymer 1998;39:801–10.

[37] Qu L, Huang G, Wang Q, Xie Z. J Polym Sci Part B Polym Phys 2008;46:72–9.
[38] Albouy PA. Polymer 2000;41:3083–6.
[39] Alexandru M, Cristea M, Cazacu M, Ioanid A, Simionescu BC. Polym Composite 2009;30:751–9.
[40] Bhattacharya M, Maiti M, Bhowmick AK. Polym Eng Sci 2009;49:81–98.
[41] Fornes TD, Paul DR. Polymer 2003;44:4993–5013.
[42] Clarson SJ, Dodgson K, Semlyen JA. Polymer 1985;26:930–4.
[43] Aranguren MI. Polymer 1998;39:4897–903.
[44] Osman MA, Atallah A, Müller M, Suter UW. Polymer 2001;42:6545–56.
[45] Modesti M, Lorenzetti A, Bon D, Besco S. Polym Degrad Stabil 2006;91:672–80.
[46] Shieh YT, Lin YS, Twu YK, Tsai HB, Lin RH. J Appl Polym Sci 2010;116:1334–41.
[47] Ki HC, Ok Park O. Polymer 2001;42:1849–61.
[48] Bilotti E, Zhang R, Deng H, Quero F, Fischer HR, Peijs T. Compos Sci Technol 2009;69:2587–95.
[49] Guth E, Gold O. Phys Rev 1938;53:322.
[50] Guth E. J Appl Phys 1945;16:20–5.
[51] Halpin JC, Kardos JL. Polym Eng Sci 1976;16:344–52.
[52] Halpin JC. J Compos Mater 1969;3:732–4.
[53] Wu YP, Jia QX, Yu DS, Zhang LQ. Polym Test 2004;23:903–9.
[54] Lewicki JP, Liggat JJ, Patel M. Polym Degrad Stabil 2009;94:1548–57.
[55] Camino G, Lomakin SM, Lazzari M. Polymer 2001;42:2395–402.
[56] Chen H, Zheng M, Sun H, Jia Q. Mat Sci Eng A 2007;445–446:725–30.
[57] Chivrac F, Pollet E, Schmutz M, Avérous L. Carbohyd Polym 2010;80:145–53.